Investigation of Motion Artifacts for Luminescence-based Transcutaneous Oxygen Wearable Device

Olivia Kendzulak*†, Naisargi Mehta*†, Ryan McSweeney*†, Parisa Saadatmand Hashemi†, and Ulkuhan Guler†
†Department of Electrical and Computer Engineering, Worcester Polytechnic Institute, Worcester, MA 01609 USA

***Abstract*—Respiratory diseases are among the top causes of mortality globally, and their effective control frequently relies on accurate monitoring of oxygen levels. The home quarantines during the COVID-19 pandemic have underscored the need for miniaturized respiratory monitoring technologies, especially in remote patient care settings. This paper presents a study on quantifying motion artifacts in a novel, wearable, noninvasive sensor. This sensor is designed to monitor transcutaneous oxygen, a marker correlated with the partial pressure of oxygen in arteries and indicative of pulmonary disease progression. It utilizes a luminescent film whose emission properties inversely correlate with oxygen levels. This study was conducted to assess the impact of motion artifacts on the sensor's accuracy, evaluating its performance under various motion conditions through three tests: dual motion, single motion, and extended motion, involving a flexible prototype with an integrated sensor and accelerometer. The test data, with no post-signal processing, demonstrated minimal impact on accuracy, with discrepancies not exceeding 0.8%. These findings highlight the wearable oxygen sensor's potential for reliable, continuous monitoring in dynamic environments, although future research could focus on solutions to further eliminate the minimal influence of motion artifacts identified in this study.**

I. Introduction

According to the World Health Organization, some respiratory illnesses (chronic obstructive pulmonary disease (COPD), lower respiratory infections, trachea, bronchus, lung cancers) are among the top ten diseases that cause death worldwide [1]. The management of these illnesses heavily relies on oxygen monitoring to track their progression. This necessity, highlighted during the COVID-19 pandemic, underscores the need for effective respiratory monitoring solutions easily deployable outside of the clinical setting [2]–[4]. As a result, remote patient monitoring emerges as a significant concern [5].

Monitoring the partial pressure of oxygen in arteries ($\mathrm{PaO_2}$) can help with the early detection of pulmonary diseases, such as COPD, COVID-19, and lower respiratory diseases [6]. A recent luminescence-based sensor [7] measures oxygen diffusing through the skin, also known as transcutaneous oxygen $\mathrm{PtcO_2}$, which is correlated with $\mathrm{PaO_2}$. This method uses a light-emitting diode (LED) to excite a luminescent sensing film, making luminophore molecules transfer from their ground energy state to a higher energy state [8]. As the luminophore molecules revert from the higher energy state, they emit light characterized by intensity and lifetime (τ). Both luminescence intensity and lifetime correlate inversely with the partial pressure of oxygen ($\mathrm{PO_2}$). Compared to intensity-based methods, the lifetime-based approach is more robust against optical path changes (i.e. motion artifacts) and excitation strength [9]. To calculate the lifetime, the light detected by a photodiode is processed through an analog front end (AFE) and converted to digital form with an analog-to-digital converter (ADC) [10]. In this paper, we explore the impact of motion artifacts on the measurements of the sensor in [7]. It is important to quantify the impact of these artifacts to better understand the reliability of this sensor in dynamic environments outside of the clinical setting.

The remainder of this paper is organized as follows. In Section II, we compare similar, light-based technologies to gain context of the significance of motion artifacts and the importance of their investigation and characterization. Section III details the experiments conducted, including setups and data collection methods. The results of these experiments are presented and discussed in Section IV. Finally, we reflect on the contributions our work makes to the field of transcutaneous oxygen sensing and consider future directions for research in Section V.

II. Background

The concern for motion artifacts stems from other light-based technologies, such as photoplethysmography (PPG), a noninvasive optical method commonly used to measure changes in blood volume to estimate oxygen saturation and heart rate, which suffers from significant deviations in measurements in the presence of motion [11]–[13]. Pankaj et al. demonstrated the necessity of computationally intensive motion artifact correction algorithms in wearable devices to make PPG data accurate and reliable for heart rate measurement [14].

Functional near-infrared spectroscopy (fNIRS) devices, used to monitor changes in the cortical layer for brain imaging by using near-infrared light, are another technology that needs motion artifact correction for improved measurement [15]–[17]. Brigadoi et al. discuss the need for motion artifact correction in fNIRS devices and Huang et al. even suggest a combination of hardware and algorithmic-based solutions [18], [19]. Given the existence of motion artifacts in similar technologies and the prevalence of complex movements and accelerations in sensors attached to an active human body, the transcutaneous oxygen monitor demands investigation to characterize the influence of motion on the wearable $\mathrm{PtcO_2}$ sensor.

Olivia Kendzulak*, Naisargi Mehta* and Ryan McSweeney* contributed equally to this work. This material is based upon work supported in part by the National Science Foundation (NSF) under Grant OAC-2203827 and the National Institute of Health (NIH) under Grant 1R01HL172293-01. Corresponding author: Ulkuhan Guler: uguler@wpi.edu.

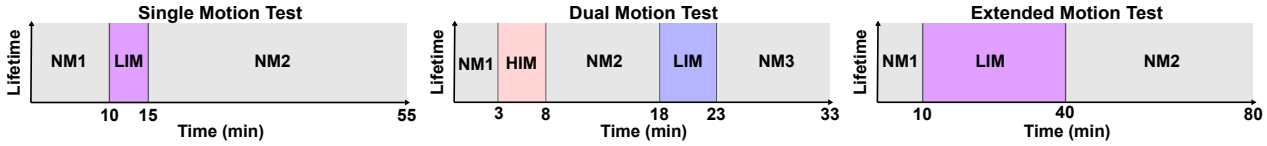

(a) (b) (c)

Fig. 1: The protocols designed for (a) single motion test, (b) dual motion test, and (c) extended motion test (motion types are denoted as NM - no motion, LIM - low-intensity motion, and HIM - high-intensity motion).

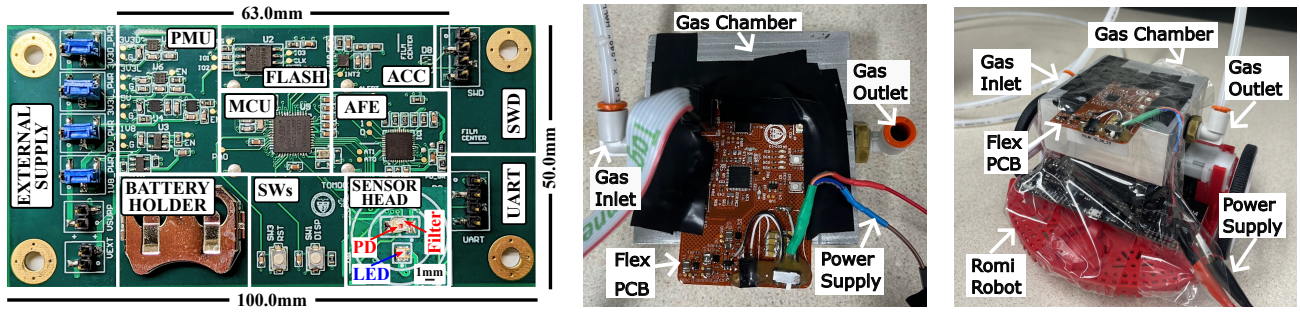

(a) (b) (c)

Fig. 2: (a) PCB prototype annotated with main circuit blocks. Motion test setups for (b) single- and dual-motion tests and (c) extended-motion test.

III. Protocol Implementation, Test Setup, and Data Collection

To accurately quantify the impact of motion on measurement accuracy, a comprehensive testing methodology has been developed to examine variations in lifetime values under different scenarios. Our approach includes three distinct test protocols, illustrated in Fig. 1, each designed to understand how motion artifacts can affect lifetime values under various conditions. Since this sensor is to be part of a wearable device, it is imperative to test various motion scenarios. The device can be used during different motion intensities as well as varying lengths of time. In addition, testing motion at various oxygen levels is crucial to analyze the varied changes in lifetime values, as the nature of the exponential decay curve of PO_2 versus lifetime, depicted in Fig. 5, implies that the alterations in lifetime values will differ for each level of PO_2 [7], [8].

The experiment setup comprises an aluminum gas chamber, within which a luminescent film is placed. Opposite this film, a flexible circuit board equipped with an accelerometer is placed. The flexible circuit board's architecture resembles the printed circuit board (PCB) with main circuit blocks, illustrated in Fig. 2a. This arrangement aims for efficient data collection by ensuring the sensor directly faces the center of the luminescent film, as illustrated in Fig. 2b. The extended motion experiment is performed by a Romi Robot controlled by a Romi 32U4 control board. The test setup from the previous experiment is used and attached to the robot, as seen in Fig. 2c.

A. Single Motion Tests at 50 mmHg Oxygen

The first protocol, 'Single Motion,' showcased in Fig. 1a, is designed for a constant PO_2 of 50 mmHg, with a single instance of motion to assess its impact on lifetime values. Selecting 50 mmHg is based on the typical PtcO2 values observed in the absence of heat application in our experiments [20]. Heating is used to increase the oxygen diffusion through the skin in the traditional transcutaneous oxygen monitors [21]. This test allows for the isolation of motion's impact on the sensor's performance, establishing a clear baseline for its responsiveness without the confounding effects of fluctuating oxygen levels.

The initial stability phase begins with a three to ten-minute period of no motion. Initially the tests were performed with three minutes in the no motion phase. However, to better visualize the baseline at the initial phase, we extended the stabilization period to ten minutes for the remaining tests. This extended duration allows the sensor to settle into the environment, ensuring that a reliable baseline for sensor readings is established without any motion influence. In the following, a five-minute motion period is introduced for assessing the sensor's response to movement, simulating potential real-life disturbances. Concluding the sequence, a 33-to-40-minute stability period follows the motion. This extended final phase is designed to observe the sensor's ability to maintain its baseline readings after experiencing motion, providing a comprehensive view of its stability over time. The experimental setup in Fig. 2b is utilized for Single Motion tests.

B. Dual Motion Tests Across Oxygen Variations

In the 'Dual Motion' protocol, motion is induced twice in a single experiment under varying PO_2. During this test, high- and low-intensity motions are tested at four different PO_2 levels. This test protocol provides insight into whether the sensor's performance is affected by consecutive disturbances, which is vital for understanding how it might perform in real-world scenarios where users are not stationary. Furthermore, testing across a range of PO_2 levels with repeated motion events allows for a detailed analysis of how oxygen variability influences the sensor's response to motion.

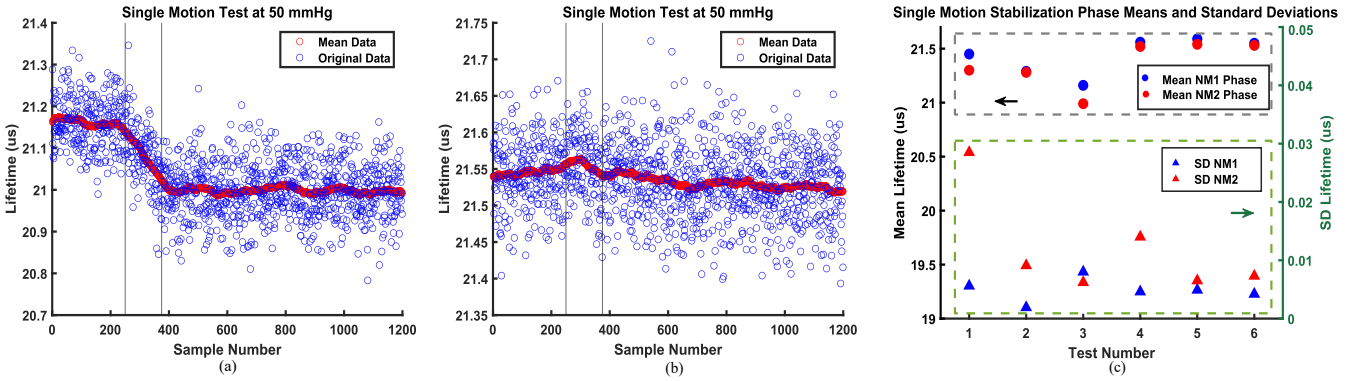

Fig. 3: (a) Single motion test with negligible change in lifetime, (b) single motion test with noticeable change in lifetime, (c) means and standard deviations for no motion phases 1 (NM1) and 2 (NM2) during single motion tests.

This experiment investigates the sensor's performance across four different PO_2 levels, from no oxygen present (0 mmHg) to a level resembling that of ambient air ($\sim$ 150 mmHg). To accurately create these specific oxygen conditions, a mixture of high-purity oxygen (OX UHP20, sourced from Airgas) and nitrogen (NI UHP80, also from Airgas) is used. The utilized experimental setup was previously elaborated in [7]. This mixture is carefully adjusted through mass flow controllers to reach the target PO_2 levels: 0 mmHg (0% O_2), 50 mmHg (6.57% O_2), 100 mmHg (13.2% O_2), and 150 mmHg (19.7% O_2). Nitrogen makes up the balance to total 760 mmHg, the standard atmospheric pressure.

To assess the influence of motion artifacts on sensor performance across the various PO_2 levels, the test sequence is designed to mimic real-world conditions where motion intensities can vary, depicted in Fig. 1b for Dual Motion tests. Each test starts with a three-minute initial no motion phase. Subsequently, this phase transitions into five minutes of high-intensity motion, followed by a ten-minute no motion interval to monitor post-motion signal behavior. Following this, a phase of low-intensity motion for five minutes is conducted before entering a concluding stabilization period of ten minutes to again monitor post-motion signal behaviour. The experimental setup in Fig. 2b is utilized for Dual Motion tests.

C. Extended Motion at 50 mmHg Oxygen

The 'Extended Motion' test is performed at 50 mmHg oxygen pressure but extends the motion duration to evaluate its prolonged effects. This is crucial for continuous monitoring applications, where the sensor must accurately track changes in oxygenation over extended periods, despite ongoing user activity. To observe the effects of a longer period of motion on the sensor, we test movement for 30 minutes, as shown in Fig. 1c. The 30 minutes of movement is performed by a Romi Robot, programmed to move back and forth 15 cm. Before the movement, there is a ten-minute stabilization period to identify the drop during the motion period. The test setup from the previous experiment is used and attached to the robot as seen in Fig. 2c. The oxygen pressure level used is 50 mmHg. This test helps us to identify the effect of motion artifacts on the signal during extended periods of motion.

TABLE I
Summary of Max Drops in Lifetime Values, Corresponding mmHg, and Percentage in Single Motion Tests

Lifetime Drop (μs)	PO_2 Drop (mmHg)	PO_2 Drop (%)
0.011	0.082	0.011
0.025	0.180	0.024
0.056	0.406	0.053
0.012	0.088	0.012
0.117	0.837	0.110
0.022	0.156	0.021
0.053	0.378	0.051
0.023	0.167	0.022

IV. Results

A. Single Motion Tests at 50 mmHg

Upon analysis of the measurement data, we observed two distinct response patterns. Notably, two tests exhibited a clear decrease in lifetime values during the motion phase, as illustrated in Fig. 3a. This contrasted with the remaining tests, which did not present a clear decline during motion periods as seen in Fig. 3b. After the motion, we observed that the signal tends to settle at a new value. The mean and standard deviations during the "No Motion" phase 1 (NM1) and "No Motion" phase 2 (NM2) are shown in Fig. 3c. The Table I shows the drops in lifetime values (μs) and the corresponding value in mmHg and percentage. Each 1% of oxygen pressure is equivalent to 7.6 mmHg. The highest drop in PO_2 is 0.11%.

B. Method to Quantify the Motion Artifacts

To quantify the effects of motion artifacts during the motion phase, the maximum drops on the mean plot (difference between maximum and minimum values during motion) were calculated. Subsequently, these drops were translated into corresponding PO_2 values in mmHg. This conversion was essential for understanding how much motion artifacts negatively influence the sensor's PO_2 readings. Based on data collected from experiments carried out at four distinct PO_2 values for the dual motion tests, Fig. 5 was created to illustrate

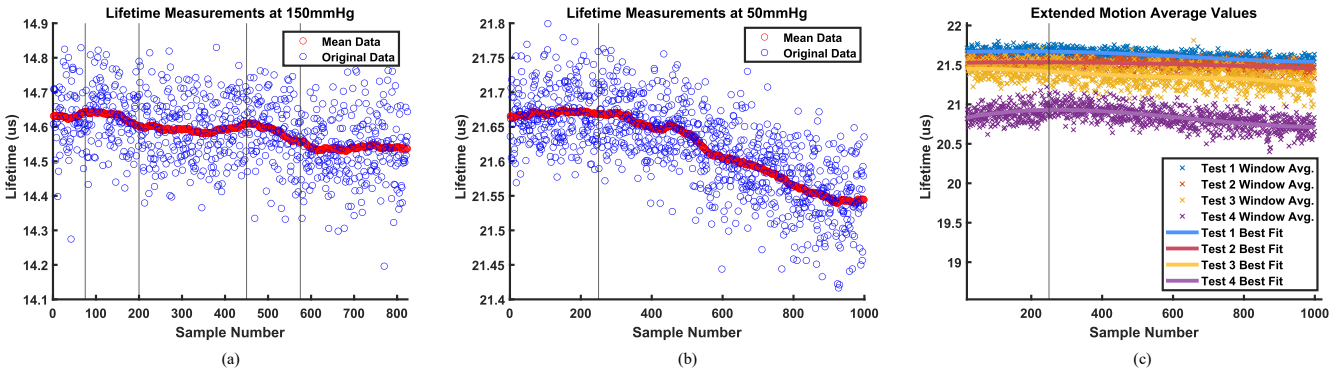

Fig. 4: (a) Dual motion test, (b) extended motion test, and (c) multiple test results with the averages of extended motion tests.

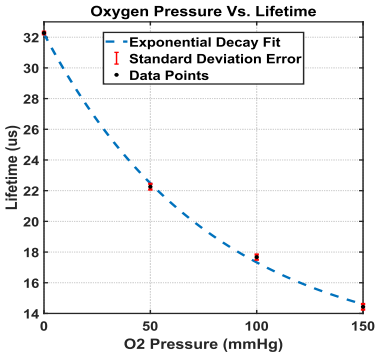

Fig. 5: Decay curve used for lifetime to PO_2 conversion.

the relation between PO_2 and lifetime values. The black data points signify the average lifetime value corresponding to each PO_2, while the red error bars illustrate the deviation in lifetime value observed during each maximum drop. The data points were fit to an exponential decay model, shown as a dashed blue line in Fig. 5, and the fit equation is given as follows:

$$\tau = 20.6905 \times e^{-0.0127x} + 11.5368, \quad (1)$$

where the variables x and τ represent PO_2 in mmHg and lifetime in μs, respectively. With this equation, we calculate the derivative at the four different PO_2 values used in the dual motion tests. The derivative is the rate of change in mmHg/μs. This rate is then used in a linear equation as the slope and maximum τ drops serve as the dependent variable. Through this approach, we can determine the maximum PO_2 drop in mmHg and the oxygen percentage from the lifetime values that the prototype measures.

C. Dual Motion Test Results

Fig. 4a illustrates an example of the signal output obtained during the dual motion test at a PO_2 of 150 mmHg. To quantitatively evaluate the extent of artifacts during dual motion experiments, we determined the maximum decrease in lifetime values during motion, observed across each oxygen level tested. These maximum drops were converted into corresponding PO_2 in Table II. It is evident from Table II that none

TABLE II
Summary of Max Drops in Lifetime Values, Corresponding mmHg, and Percentage in Dual Motion Tests

PO_2 (mmHg)	Lifetime Drop (μs)	PO_2 Drop (mmHg)	PO_2 Drop (%)
150	0.165	4.219	0.555
100	0.377	5.102	0.671
50	0.337	2.422	0.319
0	0.363	1.383	0.182

of the observed drops exceed 1% PO_2. The most substantial drop is 5.102 mmHg (0.67%), indicating that motion artifacts have a minimal effect on the PO_2 output of the sensor. In addition, the standard deviation of lifetime, represented by the error bars in Fig. 5, is not significant.

D. Extended Motion at 50 mmHg

The extended motion tests provide a similar result to the dual motion tests. In Fig. 4b, the plotted data reveals a drop during the motion period of the test that tapers off towards the end of the 30-minute motion period around 900 samples. The results from the extended motion tests are visualized in Fig. 4c. All tests were performed under the same PO_2 conditions with the same sensor film and board on different days. Cross markers represent the moving average measurements, computed with a window length of one hundred. Solid lines depict the polynomial fit with a degree of 4, serving as the line of best fit. Additionally, a vertical line at 250 samples denotes the start of the motion period. From each average test, it is evident that the slope decreases as time increases. The total drops in PO_2 values varied between 2 mmHg to about 6 mmHg with the highest value being 6.054 mmHg (0.797 %). It is evident that the longer motion does not increase the drop in lifetime and the values stop decreasing around 15 minutes.

The Food and Drug Administration (FDA) recommends that the accuracy of $PtcO_2$ should be within 5 mmHg over the range of 0 to 20.9% and 10 mmHg for the higher oxygen range [22]. The presented values in Table I are consistently lower than the values recommended by the FDA. The values in Table II are also mainly lower than 5 mmHg except one slightly higher than that value. In the extended motion tests, the $PtcO_2$ change reaches a maximum of 6.054 mmHg (0.797 %). These results indicate the robustness of the lifetime-based

measurements of luminescence-based transcutaneous oxygen prototype against motion artifacts even with the raw data without post-processing applied.

V. Conclusion

This paper has detailed efforts to quantify and understand the impact of motion artifacts on a transcutaneous oxygen measurement sensor, highlighting the pursuit of a reliable, wearable, noninvasive blood oxygen sensor. Grounded in previous research, the findings contribute significantly to the comprehension of the sensor's behavior in the presence of motion. Through the setup and execution of three experiments—dual motion, single motion, and extended motion—the resilience of this luminescence-based sensor against motion artifacts was evidenced, demonstrating less than 1% sensor error even when subjected to motion.

Compared to the motion artifacts found in other light-based technologies, such as PPG and fNIRS, the luminescence-based transcutaneous oxygen monitor with lifetime measurement technique demonstrates less vulnerability against motion artifacts. At most, the motion artifacts caused a PO_2 error of about 6 mmHg at an extended motion duration. These findings support the potential for this sensor in applications that require reliable, long-term, wearable, continuous, oxygen monitoring. Future motion artifact testing could involve long-term human testing to better quantify long-term drift and deviation and the development of motion artifact correction to further improve sensor accuracy.

VI. Acknowledgements

We would like to acknowledge Isil Isiksalan for her generous contributions in guiding and reviewing this work, as well as Vladimir Vakhter, Burak Kahraman, and Tuna Tufan for their valuable support, which greatly contributed to the success of this research.

References

[1] *World Health Organization*: The top 10 causes of death. [Online]. Available: https://www.who.int/news-room/fact-sheets/detail/the-top-10-causes-of-death

[2] U. Guler, I. Costanzo, and D. Sen, "Emerging blood gas monitors, how they can help with COVID-19," *IEEE Solid-State Circuits Magazine*, vol. 12, no. 4, pp. 33–47, 2020.

[3] M. Folke, L. Cernerud, M. Ekström, and B. Hök, "Critical review of noninvasive respiratory monitoring in medical care," *Medical and Biological Engineering and Computing*, vol. 41, no. 4, pp. 377–383, Jul. 2003.

[4] J. W. Severinghaus, P. Astrup, and J. F. Murray, "Blood Gas Analysis and Critical Care Medicine," *American Journal of Respiratory and Critical Care Medicine*, vol. 157, no. 4, pp. S114–S122, Apr. 1998, publisher: American Thoracic Society - AJRCCM.

[5] D. R. Seshadri, E. V. Davies, E. R. Harlow, J. J. Hsu, S. C. Knighton, T. A. Walker, J. E. Voos, and C. K. Drummond, "Wearable Sensors for COVID-19: A Call to Action to Harness Our Digital Infrastructure for Remote Patient Monitoring and Virtual Assessments," *Frontiers in Digital Health*, vol. 2, 2020.

[6] I. Costanzo, D. Sen, L. Rhein, and U. Guler, "Respiratory monitoring: Current state of the art and future roads," *IEEE Reviews in Biomedical Engineering*, vol. 15, pp. 103–121, 2022.

[7] V. Vakhter *et al.*, "A prototype wearable device for noninvasive monitoring of transcutaneous oxygen," *IEEE Transactions on Biomedical Circuits and Systems*, 2023.

[8] I. Costanzo, D. Sen, J. Adegite, P. M. Rao, and U. Guler, "A noninvasive miniaturized transcutaneous oxygen monitor," *IEEE Transactions on Biomedical Circuits and Systems*, vol. 15, no. 3, pp. 474–485, Jun. 2021.

[9] V. Vakhter, B. Kahraman, G. Bu, F. Foroozan, B. A. Beidleman, and U. Guler, "The Impact of Motion Artifacts on Transcutaneous Oxygen Measurements," in *2023 IEEE Biomedical Circuits and Systems Conference (BioCAS)*, Oct. 2023, pp. 1–5, iSSN: 2766-4465.

[10] B. Kahraman, V. Vakhter, I. Costanzo, G. Bu, F. Foroozan, and U. Guler, "A Miniaturized Prototype for Continuous Noninvasive Transcutaneous Oxygen Monitoring," in *2022 IEEE Biomedical Circuits and Systems Conference (BioCAS)*, Oct. 2022, pp. 486–490, iSSN: 2163-4025.

[11] D. Castaneda, A. Esparza, M. Ghamari, C. Soltanpur, and H. Nazeran, "A review on wearable photoplethysmography sensors and their potential future applications in health care," *International Journal of Biosensors & Bioelectronics*, vol. 4, no. 4, pp. 195–202, 2018.

[12] A. Temko, "Accurate Heart Rate Monitoring During Physical Exercises Using PPG," *IEEE Transactions on Biomedical Engineering*, vol. 64, no. 9, pp. 2016–2024, Sep. 2017, conference Name: IEEE Transactions on Biomedical Engineering.

[13] M. R. Ram, K. V. Madhav, E. H. Krishna, N. R. Komalla, and K. A. Reddy, "A Novel Approach for Motion Artifact Reduction in PPG Signals Based on AS-LMS Adaptive Filter," *IEEE Transactions on Instrumentation and Measurement*, vol. 61, no. 5, pp. 1445–1457, May 2012, conference Name: IEEE Transactions on Instrumentation and Measurement.

[14] Pankaj, A. Kumar, R. Komaragiri, and M. Kumar, "A Review on Computation Methods Used in Photoplethysmography Signal Analysis for Heart Rate Estimation," *Archives of Computational Methods in Engineering*, vol. 29, no. 2, pp. 921–940, Mar. 2022.

[15] R. J. Cooper, J. Selb, L. Gagnon, D. Phillip, H. W. Schytz, H. K. Iversen, M. Ashina, and D. A. Boas, "A Systematic Comparison of Motion Artifact Correction Techniques for Functional Near-Infrared Spectroscopy," *Frontiers in Neuroscience*, vol. 6, p. 147, Oct. 2012.

[16] R. Di Lorenzo, L. Pirazzoli, A. Blasi, C. Bulgarelli, Y. Hakuno, Y. Minagawa, and S. Brigadoi, "Recommendations for motion correction of infant fNIRS data applicable to multiple data sets and acquisition systems," *NeuroImage*, vol. 200, pp. 511–527, Oct. 2019.

[17] M. Kim, S. Lee, I. Dan, and S. Tak, "A deep convolutional neural network for estimating hemodynamic response function with reduction of motion artifacts in fNIRS," *Journal of Neural Engineering*, vol. 19, no. 1, p. 016017, Feb. 2022, publisher: IOP Publishing.

[18] S. Brigadoi, L. Ceccherini, S. Cutini, F. Scarpa, P. Scatturin, J. Selb, L. Gagnon, D. A. Boas, and R. J. Cooper, "Motion artifacts in functional near-infrared spectroscopy: A comparison of motion correction techniques applied to real cognitive data," *NeuroImage*, vol. 85, pp. 181–191, Jan. 2014.

[19] R. Huang, K.-S. Hong, D. Yang, and G. Huang, "Motion artifacts removal and evaluation techniques for functional near-infrared spectroscopy signals: A review," *Frontiers in Neuroscience*, vol. 16, 2022.

[20] A. Leonardi, C. Murphy, S. Hobson, V. Rohera, V. Vakhter, B. Kahraman, G. Bu, F. Foroozan, L. Rhein, and U. Guler, "Optimizing Transcutaneous Oxygen Measurement Sites on Humans," in *2023 45th Annual International Conference of the IEEE Engineering in Medicine & Biology Society (EMBC)*, Jul. 2023, pp. 1–4, iSSN: 2694-0604.

[21] W. van Weteringen, T. G. Goos, T. van Essen, C. Ellenberger, J. Hayoz, R. C. J. de Jonge, I. K. M. Reiss, and P. M. Schumacher, "Novel transcutaneous sensor combining optical tcPO2 and electrochemical tcPCO2 monitoring with reflectance pulse oximetry," *Med. Biol. Eng. Comput.*, vol. 58, no. 2, pp. 239–247, Feb 2020.

[22] "Cutaneous Carbon Dioxide (PcCO2) and Oxygen (PcO2) Monitors - Class II Special Controls Guidance Document for Industry and FDA," Dec. 2002. [Online]. Available: https://www.fda.gov/medical-devices/guidance-documents-medical-devices-and-radiation-emitting-products/cutaneous-carbon-dioxide-pcco2-and-oxygen-pco2-monitors-class-ii-special-controls-guidance-document